Mechanisms of controlled crystallization of struvite-K by NTA and EDTA sodium salt

Alberto Viani[a,*], Lucie Zárybnická[b], Radek Ševčík[b], Petra Mácová[b], Jana Machotová[c]

[a]Slovenian National Building and Civil Engineering Institute, Dimičeva ulica 12, SI-1000 Ljubljana, Slovenia

[b]Institute of Theoretical and Applied Mechanics of the Czech Academy of Sciences, Centre Telč, Prosecká 809/76, 190 00 Praha 9, Czech Republic

[c]Institute of Chemistry and Technology of Macromolecular Materials, Faculty of Chemical Technology, University of Pardubice, Studentská 573, 532 10 Pardubice, Czech Republic

*Corresponding author: Alberto Viani, e-mail: alberto.viani@zag.si;

Full mail address: Slovenian National Building and Civil Engineering Institute, Dimičeva ulica 12, SI-1000 Ljubljana, Slovenia

Tel. +386 1 2804315.

Keywords: A1. Adsorption; A1. Nucleation; B1. Phosphates; B1. Minerals

Abstract

The mechanisms by which Ethylenediaminetetraacetic acid (EDTA) and Nitrilotriacetic acid (NTA) control the precipitation of struvite-K from solution have been investigated at room temperature, pH = 9, two degrees of supersaturation, and mixing energy. The interest spans from the potassium and phosphorus recovery from wastewater, the prevention of scale deposits in wastewater treatment plants, to the inhibition of kidney stones formation and the modification of magnesium phosphate

cement reaction. Both molecules influenced the spontaneous precipitation by extending the induction time, reducing the apparent rate of crystallization and the amount of reaction product. When adding 20 mM of EDTA at a low supersaturation degree, the precipitation was almost completely inhibited, whereas, at high supersaturation, it dropped to 1.36 min^{-1} and 1.71 min^{-1} from 2.14 min^{-1} and 4.09 min^{-1}, under high and low energy of mixing, respectively. Similar behaviour was observed for NTA. The additives were found to influence the reaction path by exploiting their complexing ability in solution, thus depressing the supersaturation degree in Mg^{2+} ions with respect to struvite-K and by molecular adsorption at the forming solid surfaces, hindering nucleation and crystal growth. The adsorption processes were confirmed by the more negative zeta potential measured on the crystals (from −14.5±1.0 mV to −17.0±1.6 mV and −20.8±3.0 mV for EDTA and NTA, respectively). Besides an overall reduction in crystal size (up to 85%), owing to the increased affinity for the (101) and ($\bar{1}$01) faces alteration of the crystal habit, with a reduced elongation of the precipitated crystals (aspect ratio decreasing from 2.3 to 1.3 and 1.7 for EDTA and NTA, respectively), was produced.

1. Introduction

The interest in the controlled crystallization of struvite ($MgNH_4PO_4 \cdot 6H_2O$) and of its isostructural potassium form, struvite-K (($MgKPO_4 \cdot 6H_2O$), is manifold. They both are known to form scale deposits on pipe walls and in industrial equipment for wastewater treatment (Mohajit et al., 1989); they may also precipitate in the urinary tract as components of the infectious urinary (kidney) stones and cause damage to the renal tissue (Mclean et al., 1988). Moreover, their precipitation has been envisaged as an economically and environmentally sustainable solution for the recovery of phosphorus from wastewater, as well as from the residues of biomass incineration (Gao et al., 2018). This is a way to reduce the exploitation of natural phosphate rock deposits, driven by the increasing demand for phosphorus (Shaddel et al., 2020). The methods to favour or inhibit crystallization include the intervention on thermodynamic parameters (e.g. degree of supersaturation, temperature, pH) and

the use of additives (Kofina et al., 2007; Prywer et al., 2015; Perwitasari et al., 2017; Polat and Sayan, 2020). In the latter case, chelating agents, exhibiting the ability to sequestrate metal ions, have been found very effective in controlling struvite nucleation and crystal growth (Prywer and Olszynski, 2013; Sabbag et al., 2015; Xu et al., 2021; Viani et al., 2022b). Di-sodium EDTA ($C_{10}H_{14}N_2O_8Na_2{\cdot}2H_2O$), which is a salt of ethylenediamine tetraacetic acid (EDTA, $C_{10}H_{14}N_2O_8$), is one of the most widely employed chelating agents. It possesses higher stability and solubility with respect to neat EDTA, and keeping the metal ions in solution hinders their availability for further reaction. Consequently, in crystallization experiments, an extension of the induction time is commonly detected (Jones et al., 2007; Prywer and Olszynski, 2013). At the same time, selective adsorption at the growing crystal surfaces may occur thanks to carboxyl functional groups in the molecule, impacting the size and habit of the precipitated crystals. Similar behaviour was also observed in the case of the addition of nitrilotriacetic acid (NTA, $C_3H_6NO_6$), whose structure comprises three carboxymethyl groups - $(CH_2COOH)_2$ linked to a central N atom (Jones et al., 2006). The tri-sodium salt of NTA exhibits good solubility and affinity for solid mineral surfaces (Polettini et al., 2006), and it is an effective chelating agent for metal ions in solution (Tomita et al., 1965).

In order to gain information on the mechanisms by which EDTA and NTA control the spontaneous precipitation of struvite-K from solution, in this work, the process has been studied at room temperature and pH = 9, under different conditions of energy of mixing and concentrations of the reactants and additives. The results are expected to provide basic data for optimising the above-mentioned cycles of P and K recovery to limit the formation of scale deposits or the insurgence of infectious urinary stones. Gaining control over the crystallization of struvite-K is also of interest in the performance of magnesium phosphate cements since this phase is the main reaction product in cement. These cements find application in bioengineering as materials for bone replacement, in civil engineering as cements for fast repair of damaged structures and as a matrix for nuclear waste encapsulation (Wilson and Nicholson, 1993). The additives are employed to modulate the release of

heat and the rate of reaction in order to extend the working time of the cement (Zárybnická et al., 2022; Viani et al., 2022a). The results indicated that the observed increase in induction time, the decrease in the amount of precipitate, in the apparent crystallization rates, in the crystal size, and the changes in crystal habit are the combined effect of the complexation of ions in solution by the chelants and of their interaction with the surface of the growing crystals.

2. Experimental

2.1. Materials and methods

KH_2PO_4 (KDP) (assay 99.0%, Sigma Aldrich (Germany)) and $MgCl_2 \cdot 6(H_2O)$ (assay 99.0%, Penta (Czech Republic)) were employed for struvite-K precipitation. Two 25 mL solutions were produced, dissolving each one of the reagents in boiled deionized water and correcting the pH to 9 by dropwise addition of 9M solution of KOH and NaOH to the KDP and $MgCl_2 \cdot 6(H_2O)$ solutions, respectively. Di-sodium EDTA (assay 99.0%, Lach-Ner, s.r.o. (Czech Republic)) and tri-sodium NTA (assay >98.0%, Sigma Aldrich (Germany)) were dissolved in the KDP solution before pH correction. The precipitation was obtained by mixing the two solutions and was followed by continuous measurement of pH at the constant nominal temperature of 22 °C adopting an automatic mixing and titration unit 907 Titrando (Metrohm, Swiss), equipped with a pH probe, a thermostatically-controlled water bath and a magnetic stirrer. The experiments were conducted at two nominal stirring speeds, namely, 375 and 625 rpm. The pH meter was calibrated against ISO standard buffers. Two distinct sets of solutions with K:P:Mg molar ratio 4:4:1 were employed for each stirring speed: a first one with 50 mM of K and P, and 12.5 mM of Mg, and a second one with 100 mM of K and P, and 25 mM of Mg. The experiments have been conducted at three concentrations of each of the additives for each set of solutions and stirring speed. The experimental plan and the naming conventions adopted are reported in Table 1.

Table 1. Concentrations of the starting solutions employed in the precipitation experiments.

Sample	The concentration of chemical / mM				
	Mg	K	P	EDTA	NTA
MKP_12.5_50	12.5	50	50	0	-
MKP_25_100	25	100	100	0	-
MKP_12.5_50_EDTA3	12.5	50	50	3	-
MKP_12.5_50_EDTA6	12.5	50	50	6	-
MKP_12.5_50_EDTA12	12.5	50	50	12	-
MKP_25_100_EDTA5	25	100	100	5	-
MKP_25_100_EDTA10	25	100	100	10	-
MKP_25_100_EDTA20	25	100	100	20	-
MKP_12.5_50_NTA3	12.5	50	50	-	3
MKP_12.5_50_NTA6	12.5	50	50	-	6
MKP_12.5_50_NTA12	12.5	50	50	-	12
MKP_25_100_NTA5	25	100	100	-	5
MKP_25_100_NTA10	25	100	100	-	10
MKP_25_100_NTA20	25	100	100	-	20

2.2.Materials characterization

After each experiment, the precipitate was separated from the supernatant by filtration and washing using isopropyl alcohol, followed by drying overnight at 37 °C. The crystalline product was controlled with the X-ray powder diffraction (XRPD) method adopting a Bragg-Brentano Bruker D8 Advance diffractometer (Bruker AXS, USA). Diffracted intensities from the powdered samples have been collected on a silicon strip detector covering the angular range 5–70° 2θ with a virtual step scan of 0.0102° 2θ counting 0.25 s/step. The sample was spun at 15 rpm to increase counting statistics and minimize texture effects. Cu K_α wavelength was generated at 40 mA and 40 kV and selected with a Ni filter. The crystal structure of struvite-K was confirmed by refinement of the XRPD profile with the Rietveld method using the TOPAS 4.2 (Bruker AXS, USA) software.

A scanning electron microscope Quanta 450 FEG (FEI, Czech Republic) was adopted for the morphological analysis. The crystals were observed on carbon adhesive tape after gold coating with a 10 nm gold film under low vacuum conditions (100 Pa) at 20 kV accelerating voltage. Quantitative

information on crystal shape and size was obtained by means of image analysis of pictures collected under a Keyence VHX-6000 optical microscope (Keyence, USA) adopting the freeware ImageJ software tool. To this aim, the crystals were dispersed in isopropyl alcohol in proportion 0.01 wt.%, sonicated for 15 min, mixed on a vortex mixer and then deposited on a glass plate. The images were collected at a magnification of 200×.

A Litesizer 500 instrument (Anton Paar, Austria) was employed to measure the zeta potential (ξ) of mineral particles on selected samples by dynamic light scattering. The experiments were conducted at 25 °C by dispersing 0.1 wt.% of solid in water. Results have been reported as an average of 6 replicates.

Hyperquad HYSS software (Alderighi et al., 1999) was adopted to simulate ion speciation in solution and produce distribution diagrams.

3. Results and discussion

During struvite-K precipitation, the pH decreases quickly in the first minutes to approach a plateau later on. Typical time-evolution curves are illustrated in Fig. 1. This trend has been described considering the precipitation of struvite-K, according to the reaction in *Eq.* 1 (Viani et al., 2022b):

$$Mg^{2+} + K^{+} + H_nPO_4^{n\,-3} + 6H_2O \rightarrow MgKPO_4{\cdot}6H_2O + nH^{+} \qquad (Eq.\ 1)$$

As shown in other crystallization experiments of the struvite family crystals (Bayuseno et al., 2020; Viani et al., 2022b), the change in concentration of H^+ ions is related to the rate of formation of the magnesium phosphate crystals, as detailed in the Supplementary Material. In fact, it is expected that this process dominates in the range of pH observed during the experiment since EDTA should be in the deprotonated form HL^{-3} and NTA in the form HL^{-2} (as illustrated by the distribution diagrams in the Supplementary Material Fig. S1). Moreover, the stable phosphate form is HPO_4^{2-}, which means

that in *Eq.* 1 $n = 1$. It follows that the apparent crystallisation rate can be obtained from the time-evolution of pH, assuming a kinetic model. Several kinetic experiments on struvite and struvite-K indicated that the first-order kinetic model, as expressed by *Eq.* 2, is adequate to describe the process (Ohlinger et al., 2000; Quintana et al., 2005; Bayuseno et al., 2020; Viani et al., 2022b):

$$-\frac{dC}{dt} = k(C - C_{eq}) \qquad (Eq.\ 2)$$

Where C is the virtual molar concentration of Mg^{2+} ions in solution at any time t (min), C_{eq} is the molar concentration at equilibrium. The rate constant (k) has been obtained through a nonlinear fit of the pH *vs* time curves, as illustrated in Fig. 1.

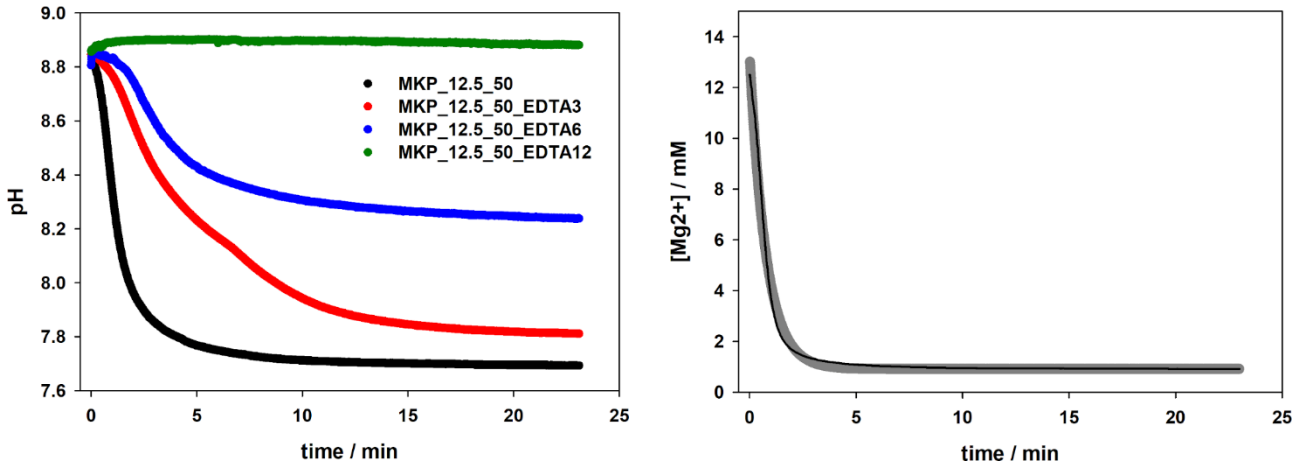

Figure 1. pH vs time curves for the samples at different EDTA content (left) at slow stirring speed. The nonlinear fit of the first-order reaction model to the kinetic curve for the sample MKP_12.5_50 (right).

The results, reported in Table 2, indicate that the energy of mixing increases the rates under the same conditions; a similar trend is observed for the degree of supersaturation (i.e. increase in the concentration of the reactants). As previously observed in precipitation in the presence of citric acid, the latter effect is enhanced at lower stirring speed (Viani et al., 2022b).

When the samples without additive are considered, the rates are in line with recent precipitation experiments of struvite-K under analogous conditions (Viani et al., 2022b), whereas they are lower with respect to other results of crystallization from synthetic urine at pH = 9 (Zhang et al., 2018). This difference may be explained by the different ionic strengths of the solution and the supersaturation degree attained.

The introduction of the additives had a remarkable effect on the rates, namely, a progressive decrease increasing their concentration. Moreover, the appearance of an induction time, indicated by the nearly flat shape of the first part of the curves, points to a delayed onset of struvite-K crystallization (Fig. 1 left). This induction time is more evident when the supersaturation level and the energy of mixing are lower and is extended in reason of the concentration of additive, as previously observed in precipitation experiments of crystals of the struvite family (Ohlinger et al., 1999; Rahaman et al., 2008). Carboxyl group-containing compounds have been reported to produce the same effect (Kofina et al., 2007; Viani et al., 2022b). Notably, compared to NTA, EDTA is more effective since the induction time is longer and the rates are, in general, lower. The inhibition of struvite-K precipitation reaches its maximum for the samples MKP_12.5_50_EDTA12, for which the kinetic parameters could not be determined, in agreement with the almost flat behaviour of the pH vs time curve illustrated in Fig. 1.

This trend can be explained by considering the solution chemistry of the additives. The degree of protonation of EDTA and NTA depends on solution pH, as illustrated in the speciation diagrams reported in Supplementary Material Fig. S1. When other cations are present, this also changes because of the formation of complexes with the molecules. As shown in Fig. 2 and Supplementary Material Fig. S2, at pH 9, the Mg^{2+} ion is complexed by EDTA in the form of LMg^{2-}, where L is the fully deprotonated form of the ligand and in the form of LMg^{-} when considering NTA. At the highest concentration of additive for each one of the two sets of experiments, almost all the Mg^{2+} is virtually

subtracted. This explains the almost flat behaviour of the corresponding pH vs time curves, which impaired the calculation of the precipitation rates.

Table 2. Results of kinetic analysis of the precipitation reaction using the first-order model at slow (375 rpm) and fast (625 rpm) stirring speed.

Sample	Slow stirring k / min^{-1}	R^2	Fast stirring k / min^{-1}	R^2
MKP_12.5_50	1.307±0.004	0.986	3.88±0.02	0.986
MKP_12.5_50_EDTA3	0.374±0.001	0.994	2.10±0.01	0.988
MKP_12.5_50_EDTA6	0.365±0.001	0.980	1.57±0.01	0.973
MKP_12.5_50_EDTA12	n.d.	n.d	n.d.	n.d.
MKP_12.5_50_NTA3	1.056±0.003	0.984	2.90±0.01	0.981
MKP_12.5_50_NTA6	0.955±0.003	0.984	1.46±0.01	0.983
MKP_12.5_50_NTA12	0.538±0.002	0.949	0.564±0.003	0.929
MKP_25_100	2.145±0.003	0.998	4.09±0.01	0.996
MKP_25_100_EDTA5	1.983±0.003	0.998	3.56±0.01	0.980
MKP_25_100_EDTA10	1.541±0.004	0.997	2.91±0.02	0.956
MKP_25_100_EDTA20	1.360±0.010	0.892	1.71±0.01	0.978
MKP_25_100_NTA5	1.960±0.004	0.997	3.78±0.02	0.979
MKP_25_100_NTA10	1.408±0.001	0.957	3.63±0.01	0.988
MKP_25_100_NTA20	1.047±0.004	0.984	1.99±0.01	0.984

Along with complexation in solution, the ability to be adsorbed at solid matrices has been reported for both molecules (Polettini et al., 2006; Hentrich et al., 2017). In Ca-carbonates, this mechanism has been considered to impair crystal growth (Wada et al., 2001; Reddy and Hoch, 2001) and the growth of nuclei of critical size (Westin and Rasmuson, 2005), with a direct impact on the rates and on the induction times. Adsorption effects have been recognized to exert control on the morphological changes observed in the product of precipitation experiments of sulphates, Ca-carbonates and Ca-phosphates in the presence of NTA and EDTA (Gopi et al., 2015)(Jones et al., 2006). At pH = 9, EDTA should be adsorbed in the form LH^{3-}, whereas NTA is largely in the form LH^{2-}. However, since

in the NTA molecule, the proton is expected to be in nitrogen, the three carboxylate groups are fully deprotonated.

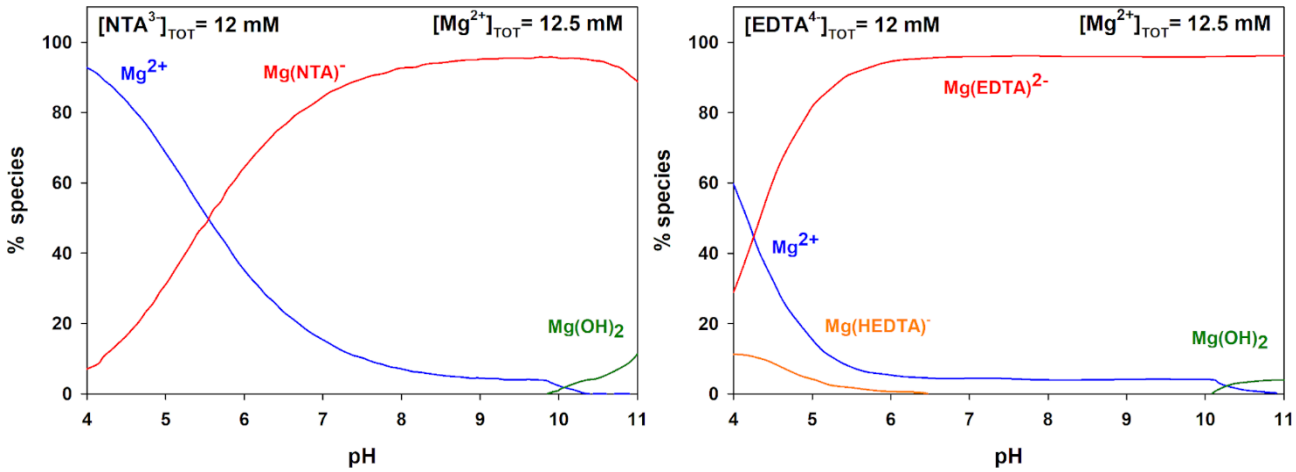

Figure 2. Distribution diagrams of Mg^{2+} and EDTA, and Mg^{2+} and NTA species as a function of pH at 12.5 mM of Mg^{2+} ions and 12 mM of ligands, as indicated.

Therefore, upon adsorption of the negatively charged COO^- ion, the mineral surface assumes more negative values of ξ (Kallay and Matijevic, 1985; Mudunkotuwa and Grassian, 2010). Because of its robustness and ease of use, the dynamic light scattering method, based on simple theoretical models, is routinely adopted for the measurement of ξ, although a number of factors may affect the results (Delgado et al., 2007). Of relevance for the present case are the differences in the predominant crystal shape between samples and the significant deviations from the spherical particle shape. For this reason, the measurements have been limited to three samples obtained by precipitation at slow stirring speed, namely, MKP_12.5_50, MKP_12.5_50_EDTA6 and MKP_12.5_50_NTA6. The measured values of ξ were −14.5±1.0 mV, −17.0±1.6 mV, −20.8±3.0 mV, respectively. The ξ for the struvite-K precipitated without additives is in line with previously published ones (Polat and Eral, 2022; Viani et al., 2022b). At this additive concentration, the effect on ξ of the additives seems rather small. However, it is higher than what was recently reported for struvite-K synthesized in the presence of 20 mM of citric acid (Viani et al., 2022b). In any case, the more negative values are in agreement

with the adsorption of both additives on the crystal faces. The difference between MKP_12.5_50_NTA6 and MKP_12.5_50_EDTA6 is within the standard deviation of the measurements. There is a correlation between the zeta potential values and the particle size values, with smaller particles having a larger surface area and therefore more negative zeta potential values (Simunkova et al., 2009).

When the absolute values of ξ are considered, it must be noted that they indicate relatively unstable suspensions with a tendency to agglomeration. In fact, the threshold for agglomeration is considered −15 mV, but a stable suspension of particles must possess ξ lower than −30 mV (Delgado et al., 2007). The Rietveld refinements of XRPD patterns indicated a good agreement with the structure model of struvite-K, as exemplified in Fig S3, reported as Supplementary Material.

The morphology of the precipitated crystals, as viewed under SEM, is illustrated in Fig. 2-4. In agreement with the results of kinetic analysis, the crystals which formed at high stirring speed are, on average, bigger. The individuals precipitated in the absence of additives were frequently dendritic or exhibited the characteristic X-shaped twinning (Fig. 3e). These morphologies were commonly observed at high growth rates in crystals of the struvite family (Abbona and Boistelle, 1979; Wang et al., 1993; Viani et al., 2022b). On the contrary, the needle-like crystals, which were obtained during the precipitation of struvite-K for nutrient recovery (Gao et al., 2018; Zhang et al., 2018), were not reproduced in our case. The reason likely resides in the more extreme conditions attained during those batch experiments. At higher precipitation rates, cyclic twinning was also frequently observed (Fig. 4). According to the typical struvite-K crystal habit, sketched in Fig. 5, the (001) faces were, in this case, more expressed.

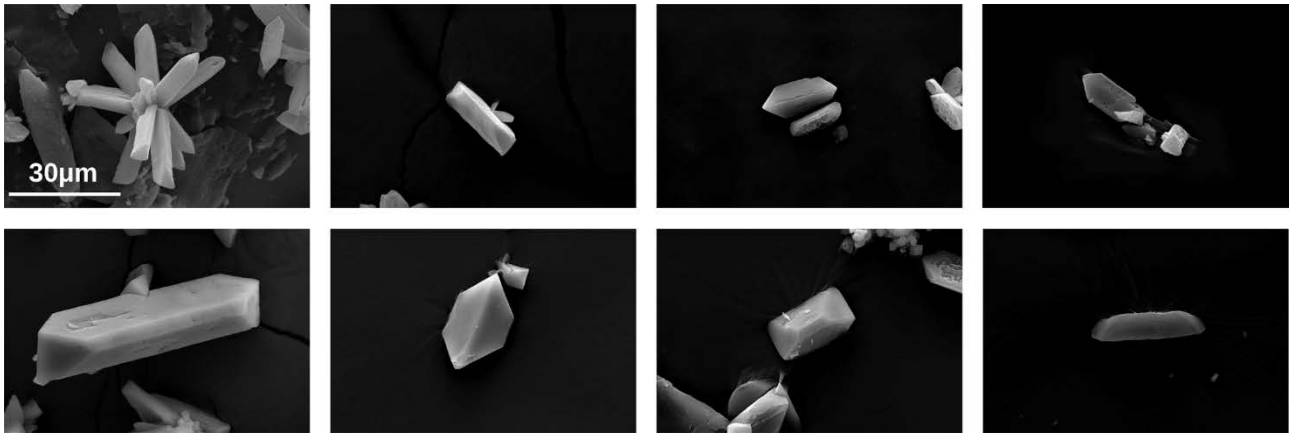

Figure 2. SEM micrographs at the same magnification of struvite-K precipitated at increasing amounts of EDTA at two stirring speeds. MKP_12.5_50, a, e; MKP_12.5_50_EDTA3, b, f; MKP_12.5_50_ EDTA 6, c, g; MKP_12.5_50_ EDTA 12, d, h. Slow stirring speed: a-d, fast stirring speed: e-h.

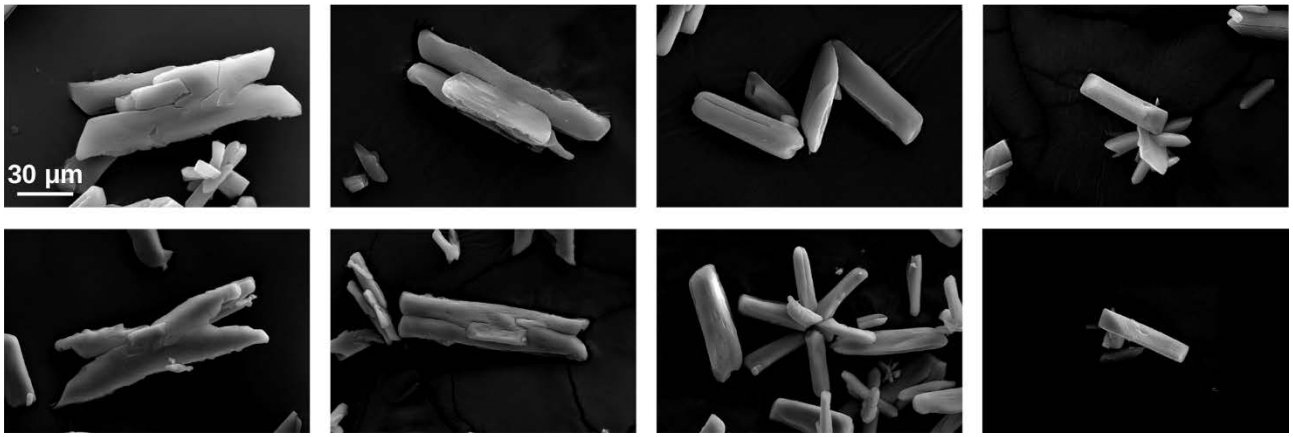

Figure 3. SEM micrographs at the same magnification of struvite-K precipitated at increasing amounts of EDTA at two stirring speeds. MKP_25_100, a, e; MKP_25_100_EDTA5, b, f; MKP_25_100_ EDTA10, c, g; MKP_25_100_ EDTA20, d, h. Slow stirring speed: a-d, fast stirring speed: e-h.

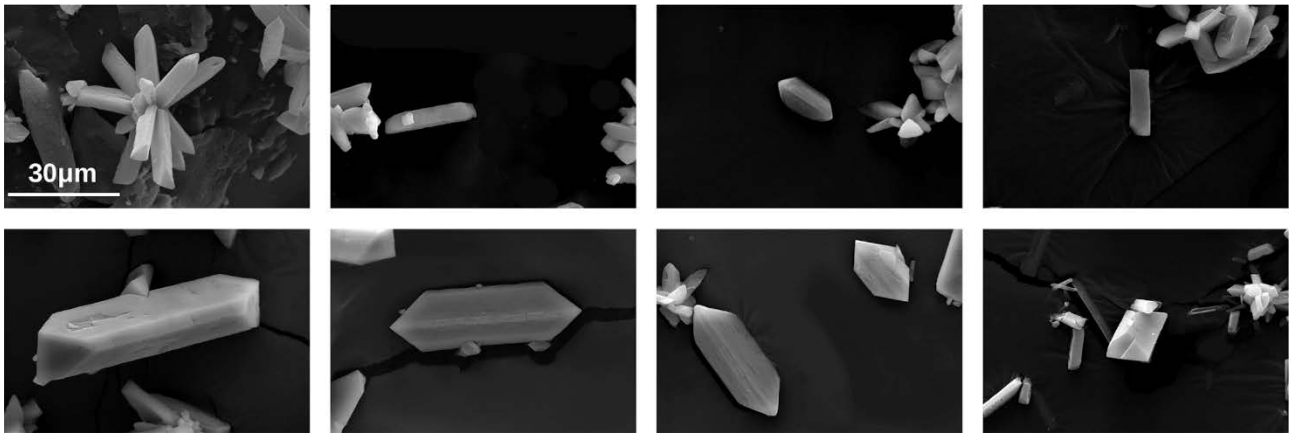

Figure 3. SEM micrographs at the same magnification of struvite-K precipitated at increasing amounts of NTA at two stirring speeds. MKP_12.5_50, a, e; MKP_12.5_50_NTA3, b, f; MKP_12.5_50_NTA6, c, g; MKP_12.5_50_NTA12, d, h. Slow stirring speed: a-d, fast stirring speed: e-h.

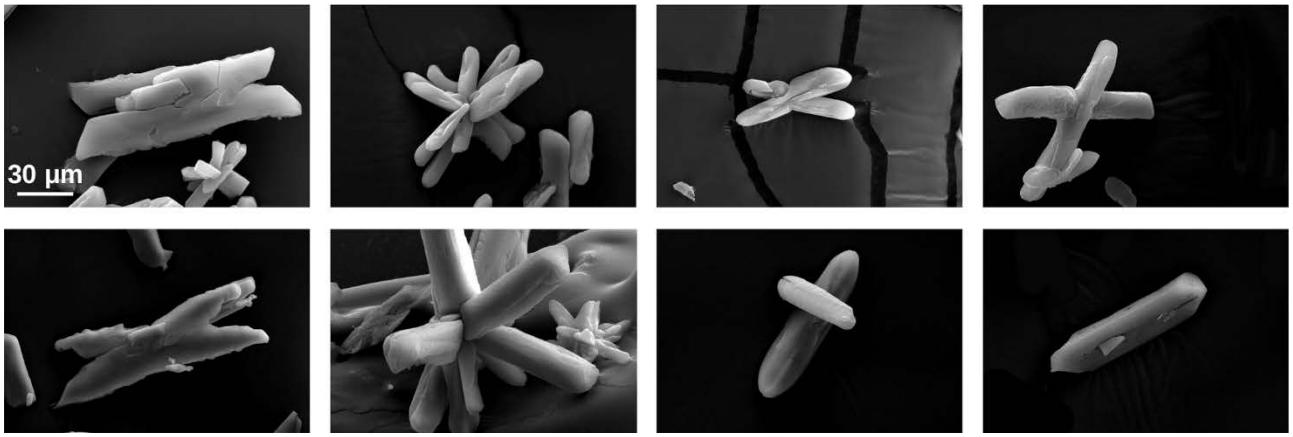

Figure 4. SEM micrographs at the same magnification of struvite-K precipitated at increasing amounts of NTA at two stirring speeds. MKP_25_100, a, e; MKP_25_100_NTA5, b, f; MKP_25_100_NTA10, c, g; MKP_25_100_NTA20, d, h. Slow stirring speed: a-d, fast stirring speed: e-h.

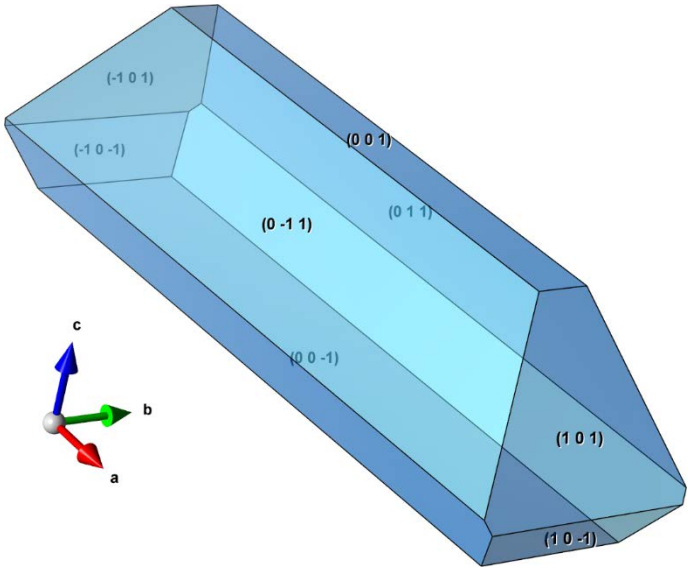

Figure 5. Schematic representation of the common crystal habit of struvite-K crystals with some of the faces indexed.

The increase in the amount of both additives induced a progressive decrease in crystal size. Moreover, some morphological changes were detected. These effects were enhanced at lower supersaturation levels (Fig. 1 and 3), where the nucleation was also more effectively inhibited. An overall reduction in crystal elongation, with individuals larger along the *a*-axis and shorter along the *b*-axis, was obtained. The reduced length along the (001) with a more expressed (101) and ($\bar{1}$01) faces frequently led to the coffin-lid morphology illustrated in Fig. 2g.

These effects have been confirmed quantitatively by analysing crystals with the aid of the tools for image analysis (Fig. S4). Table 3 summarizes relevant results of particle size distribution and shape of precipitates obtained at slow stirring speed, the group of samples less affected by the agglomeration effects mentioned above. Although these effects, along with the presence of twinning, may have biased the results to some extent, a progressive decrease in D_{50} (that is, the medium value of the particle size distribution or the diameter at 50% in the cumulative distribution) is apparent in both sets of samples. This trend towards a decrease in crystal size can also be appreciated in the particle size distribution plots, reported in Supplementary Material Fig. S5. In addition, the reduced

elongation observed under SEM is compatible with the progressive decrease in the median value of the aspect ratio (defined in the software as the ratio between the major and minor axis of the particle's fitted ellipse).

Table 3. Results of image analysis on samples precipitated under slow stirring speed.

Sample	Amount/ g	D_{50} / µm	Aspect ratio
MKP_12.5_50	0.055	17.6	1.6
MKP_12.5_50_EDTA3	0.018	16.1	1.3
MKP_12.5_50_EDTA6	0.007	12.4	1.4
MKP_12.5_50_EDTA12	n.d.	n.d.	n.d.
MKP_12.5_50_NTA3	0.048	16.4	1.5
MKP_12.5_50_NTA6	0.043	5.4	1.3
MKP_12.5_50_NTA12	0.024	5.6	1.5
MKP_25_100	0.158	26.7	2.3
MKP_25_100_EDTA5	0.125	20.2	2.3
MKP_25_100_EDTA10	0.098	4.4	1.3
MKP_25_100_EDTA20	0.027	4.4	1.3
MKP_25_100_NTA5	0.150	25.1	2.3
MKP_25_100_NTA10	0.131	19.9	2.0
MKP_25_100_NTA20	0.089	12.8	1.7

The formation of complexes in solution reduced the apparent supersaturation with respect to the complexed ions, extending the induction time, as recently documented during the precipitation of struvite-K (Viani et al., 2022b). The sequestration of Mg^{2+} ions explained the progressive decrease in the amount of precipitated struvite-K when the amount of additive was increased (Table 3). The extreme case is the sample MKP_12.5_50_EDTA12 synthesized at a slow stirring speed, for which the amount of precipitate was too low to be quantified.

Both EDTA and NTA host one adsorption site per molecule, therefore, at their higher concentration, the additives can virtually sequestrate almost all the Mg^{2+} ions in solution (see Fig. 2). However, the

results indicate that EDTA is a more effective reaction modifier than NTA; this is in agreement with comparative reports showing higher complexation ability for EDTA, owing to the higher stability of its hexadentate Mg chelates respect to the tetradentate complexes of NTA (Sabbag et al., 2015)(Neto et al., 2014).

However, it might be argued that also surface interaction effects contributed to inhibiting the amount of precipitate, similar to what was observed during the synthesis of carbonates and phosphates when adding carboxylate-containing moieties (Tobler et al., 2015; Chatzipanagis et al., 2016). Moreover, surface adsorption may result in delayed nucleation by hindering the integration of ions to form stable nuclei, as proposed for sulphates in the presence of EDTA and NTA (Jones et al., 2007)(Jones et al., 2006). In addition, in these cases, as well as during precipitation experiments of Ca-carbonates (Reddy and Hoch, 2001), Ca-phosphates (Tenhuisen and Brown, 1994; Bohner et al., 1996; López-Macipe et al., 1998; Fukuda et al., 2017) and struvite (Kofina et al., 2007; Prywer et al., 2015; Perwitasari et al., 2017; Polat and Sayan, 2020), adsorption at the surface of the growing crystals was also active, and induced alteration of the crystal shape. As reported in Table 3 and illustrated in Fig. 2-4, the extent of size and shape modifications is enhanced by the increase in the amount of additives, confirming the onset of adsorption processes. The prevalent reduced elongation with the more expressed (101) and ($\bar{1}$01) faces suggested them as a candidate for the adsorption of the additives, in analogy with previous results of struvite crystallization in the presence of phosphocitrate (Wierzbicki et al., 1997). In fact, preferential molecule adsorption at a specific crystal face causes that face to be more expressed. The selective adsorption was found to agree with the molecular modelling simulations and the indication that these planes exhibit a high density of Mg ions, resulting in a higher residual positive charge, providing an ideal local environment for the adsorption of the negatively charged molecules of the additives. The bidentate bridging or bidentate chelating were found to be by far the most favourable modes of adsorption for both moieties (Jones et al., 2007)(Jones et al., 2006).

The control exerted on the precipitation reaction by adsorption at the surface of the forming solids may occur very early since homogeneous nucleation is assumed to be preceded by the formation of pre-nucleation clusters (Navrotsky, 2004), and additives have already been proposed to be effectively adsorbed at this reaction stage (Westin and Rasmuson, 2005). The decrease in the amount of struvite-K and the size of crystals are the results of the interplay between these two processes. It may be argued that also the decrease in the R^2 values of the fit to the first-order kinetics equation (Table 2), increasing the amount of additives, is related to their intervention. In analogy with similar precipitation experiments of struvite and struvite-K in the presence of carboxyl groups (Perwitasari et al., 2017; Bayuseno et al., 2020)(Viani et al., 2022b), this highlights the progressive inadequacy of the single-step first-order reaction model, indicating that more advanced approaches, which are outside of the scope of the present study, are required to describe the system.

Also, the interpretation of the kinetic results in terms of a thermodynamic driving force for nucleation and growth is, at best, only semi-quantitative since parameters like the interfacial energy are values averaged over all the surfaces and crystal faces which form during the process (Westin and Rasmuson, 2005). They are calculated according to models assuming surfaces are smooth and in equilibrium, and these conditions are violated just because of the adsorption of the additives, which impair the integration of ions on the surface, increasing its roughness. Moreover, agglomeration, which has been observed to some extent in the precipitates with both moieties, may play a role in forming particles of detectable size, calling for adopting more complex models. Likewise, a rigorous description of the mechanisms by which additives influence nucleation and the stability of pre-nucleation clusters is not available (Westin and Rasmuson, 2005; Chatzipanagis et al., 2016).

4. Conclusions

In this work, results of precipitation experiments of struvite-K from solution at two degrees of supersaturation, two values of energy of mixing, 22°C and pH 9, in the presence of EDTA and NTA, have been reported.

- Both additives were found to reduce the apparent rates of precipitation, which dropped from 1.307 to 0.538 min^{-1} and from 3.88 to 0.564 min^{-1} at slow and fast stirring speed, respectively, adding 12 mM of NTA at low supersaturation, from 2.145 to 1.047 min^{-1} and from 4.09 to 1.99 min^{-1}, adding 20 mM of NTA at high supersaturation. EDTA had a higher impact on the rates at low supersaturation, so the rates were virtually 0 min^{-1}. At high supersaturation, the values were 1.360 min^{-1} and 1.71 min^{-1} for slow and fast stirring speeds, respectively.
- In all the samples, including the control, the rates decreased, decreasing the mixing energy (i.e. stirring speed) and degree of supersaturation.
- The induction time was always increased by the presence of the additives, to a higher extent when the amount of the additives increased and when the energy of mixing and supersaturation degree decreased.
- The amount of precipitated struvite-K was found to decrease, increasing the content of additives. In the case of synthesis under a lower supersaturation degree, with the highest content in EDTA (20 mM), the precipitation was virtually totally inhibited, whereas for NTA, under the same conditions, the reduction ranged between 44 and 83 % at low and high supersaturation degree, respectively.
- The introduction of both EDTA and NTA led to a progressive reduction in crystal size and, concomitantly, to a reduction in the maximum length of the crystals along the (001) direction. This was quantified by determining the median aspect ratio, which decreased from 2.3 to 1.3 and 1.7, at high supersaturation and slow stirring speed, for EDTA and NTA, respectively.
- The mechanisms controlling the precipitation reaction and the changes in crystal size and crystal habit were identified in the combination of sequestration of Mg^{2+} ions in solution,

owing to the chelating ability of the additives and their adsorption at the newly formed surfaces.

- The latter mechanism is likely to occur at the early stages of the reaction, inhibiting the integration of lattice ions on the forming nuclei or even the pre-nucleation clusters, inhibiting their growth, as well as during crystal growth.
- The prevalence of the shapes with (101) and ($\bar{1}$01) faces more expressed and (001) less expressed indicated the former as preferential surfaces for adsorption.
- Confirmation of the onset of surface adsorption effects on struvite-K was provided by the more negative values of ξ (from −14.5±1.0 mV to −17.0±1.6 mV and −20.8±3.0 mV, for the control sample, the sample precipitated in the presence of EDTA and NTA, respectively).

Acknowledgments

The authors acknowledge support from the Institute of Theoretical and Applied Mechanics (RVO 68378297).

References

Abbona F. and Boistelle R. (1979) Growth morphology and crystal habit of struvite crystals (MgNH4PO4·6H2O). *J. Cryst. Growth* **46**, 339–354.

Alderighi L., Gans P., Ienco A., Peters D., Sabatini A. and Vacca A. (1999) Hyperquad simulation and speciation (HySS): a utility program for the investigation of equilibria involving soluble and partially soluble species. *Coord. Chem. Rev.* **184**, 311–318.

Bayuseno A. P., Perwitasari D. S., Muryanto S., Tauviqirrahman M. and Jamari J. (2020) Kinetics and morphological characteristics of struvite (MgNH4PO4.6H2O) under the influence of maleic acid. *Heliyon* **6**, e03533.

Bohner M., Lemaitre J. and Ring T. A. (1996) Effects of Sulfate, Pyrophosphate, and Citrate Ions on the Physicochemical Properties of Cements Made of beta-Tricalcium Phosphate-Phosphoric Acid-Water Mixtures. *J. Am. Ceram. Soc.* **79**, 1427–1434.

Chatzipanagis K., Iafisco M., Roncal-Herrero T., Bilton M., Tampieri A., Kröger R. and Delgado-López J. M. (2016) Crystallization of citrate-stabilized amorphous calcium phosphate to nanocrystalline apatite: a surface-mediated transformation. *CrystEngComm* **18**, 3170–3173.

Delgado A. V., González-Caballero F., Hunter R. J., Koopal L. K. and Lyklema J. (2007) Measurement and interpretation of electrokinetic phenomena. *J. Colloid Interface Sci.* **309**, 194–

224.

Fukuda N., Tsuru K., Mori Y. and Ishikawa K. (2017) Effect of citric acid on setting reaction and tissue response to β -TCP granular cement. *Biomed. Mater.* **12**, 015027.

Gao Y., Liang B., Chen H. and Yin P. (2018) An experimental study on the recovery of potassium (K) and phosphorous (P) from synthetic urine by crystallization of magnesium potassium phosphate. *Chem. Eng. J.* **337**, 19–29.

Gopi S. P., Palanisamy K. and Subramanian V. K. (2015) Effect of NTA and temperature on crystal growth and phase transformations of CaCO 3. *Desalin. Water Treat.* **54**, 316–324.

Hentrich D., Tauer K., Espanol M., Ginebra M.-P. and Taubert A. (2017) EDTA and NTA Effectively Tune the Mineralization of Calcium Phosphate from Bulk Aqueous Solution. *Biomimetics* **2**, 24.

Jones F., Jones P., Ogden M. I., Richmond W. R., Rohl A. L. and Saunders M. (2007) The interaction of EDTA with barium sulfate. *J. Colloid Interface Sci.* **316**, 553–561.

Jones F., Oliveira A., Rohl A. L., Ogden M. I. and Parkinson G. M. (2006) Understanding the mechanism by which nitrilotriacetic acid interacts with precipitating barium sulfate. *CrystEngComm* **8**, 869.

Kallay N. and Matijevic E. (1985) Adsorption at solid/solution interfaces. 1. Interpretation of surface complexation of oxalic and citric acids with hematite. *Langmuir* **1**, 195–201.

Kofina A. N., Demadis K. D. and Koutsoukos P. G. (2007) The Effect of Citrate and Phosphocitrate On Struvite Spontaneous Precipitation. *Cryst. Growth Des.* **7**, 2705–2712.

López-Macipe A., Gómez-Morales J. and Rodríguez-Clemente R. (1998) The Role of pH in the Adsorption of Citrate Ions on Hydroxyapatite. *J. Colloid Interface Sci.* **200**, 114–120.

Mclean R. J. C., Nickel J. C., Cheng K. J., Costerton J. W. and Banwell J. G. (1988) The ecology and pathogenicity of urease-producing bacteria in the urinary tract. *Crit. Rev. Microbiol.* **16**, 37–79.

Mohajit, Bhattarai K. K., Taiganides E. P. and Yap B. C. (1989) Struvite deposits in pipes and aerators. *Biol. Wastes* **30**, 133–147.

Mudunkotuwa I. A. and Grassian V. H. (2010) Citric Acid Adsorption on TiO 2 Nanoparticles in Aqueous Suspensions at Acidic and Circumneutral pH: Surface Coverage, Surface Speciation, and Its Impact on Nanoparticle−Nanoparticle Interactions. *J. Am. Chem. Soc.* **132**, 14986–14994.

Navrotsky A. (2004) Energetic clues to pathways to biomineralization: precursors, clusters, and nanoparticles. *Proc. Natl. Acad. Sci.* **101**, 12096–12101.

Neto I. F. F., Pinto I. S. S., Barros M. T., Maycock C. D. and Soares H. M. V. M. (2014) Study of the performance of nitrilotriacetic acid and ethylenediiminopropanedioic acid as alternative biodegradable chelating agents for pulp bleaching. *Int. J. Environ. Res.* **8**, 613–620.

Ohlinger K. N., P.E., Young T. M. and Schroeder E. D. (1999) Kinetics Effects on Preferential Struvite Accumulation in Wastewater. *J. Environ. Eng.* **125**, 730–737.

Ohlinger K. N., Young T. M. and Schroeder E. D. (2000) Postdigestion Struvite Precipitation Using a Fluidized Bed Reactor. *J. Environ. Eng.* **126**, 361–368.

Perwitasari D. S., Edahwati L., Sutiyono S., Muryanto S., Jamari J. and Bayuseno A. P. (2017) Phosphate recovery through struvite-family crystals precipitated in the presence of citric acid: mineralogical phase and morphology evaluation. *Environ. Technol.* **38**, 2844–2855.

Polat S. and Eral H. B. (2022) Effect of hyaluronic acid on the struvite crystallization: A structural, morphological, and thermal analysis study. *J. Cryst. Growth* **592**, 126734.

Polat S. and Sayan P. (2020) Preparation, characterization and kinetic evaluation of struvite in various carboxylic acids. *J. Cryst. Growth* **531**, 125339.

Polettini A., Pomi R., Rolle E., Ceremigna D., De Propris L., Gabellini M. and Tornato A. (2006) A kinetic study of chelant-assisted remediation of contaminated dredged sediment. *J. Hazard. Mater.* **137**, 1458–1465.

Prywer J., Mielniczek-Brzóska E. and Olszynski M. (2015) Struvite crystal growth inhibition by trisodium citrate and the formation of chemical complexes in growth solution. *J. Cryst. Growth* **418**, 92–101.

Prywer J. and Olszynski M. (2013) Influence of disodium EDTA on the nucleation and growth of struvite and carbonate apatite. *J. Cryst. Growth* **375**, 108–114.

Quintana M., Sánchez E., Colmenarejo M. F., Barrera J., García G. and Borja R. (2005) Kinetics of phosphorus removal and struvite formation by the utilization of by-product of magnesium oxide production. *Chem. Eng. J.* **111**, 45–52.

Rahaman M. S., Ellis N. and Mavinic D. S. (2008) Effects of various process parameters on struvite precipitation kinetics and subsequent determination of rate constants. *Water Sci. Technol.* **57**, 647–654.

Reddy M. M. and Hoch A. R. (2001) Calcite Crystal Growth Rate Inhibition by Polycarboxylic Acids. *J. Colloid Interface Sci.* **235**, 365–370.

Sabbag H., Brenner A., Nikolski A. and Borojovich E. J. C. (2015) Prevention and control of struvite and calcium phosphate precipitation by chelating agents. *Desalin. Water Treat.* **55**, 61–69.

Shaddel S., Grini T., Andreassen J.-P., Østerhus S. W. and Ucar S. (2020) Crystallization kinetics and growth of struvite crystals by seawater versus magnesium chloride as magnesium source: towards enhancing sustainability and economics of struvite crystallization. *Chemosphere* **256**, 126968.

Simunkova H., Pessenda-Garcia P., Wosik J., Angerer P., Kronberger H. and Nauer G. E. (2009) The fundamentals of nano-and submicro-scaled ceramic particles incorporation into electrodeposited nickel layers: Zeta potential measurements. *Surf. Coatings Technol.* **203**, 1806–1814.

Tenhuisen K. S. and Brown P. W. (1994) The effects of citric and acetic acids on the formation of calcium-deficient hydroxyapatite at 38 C. *J. Mater. Sci. Mater. Med.* **5**, 291–298.

Tobler D. J., Rodriguez-Blanco J. D., Dideriksen K., Bovet N., Sand K. K. and Stipp S. L. S. (2015) Citrate Effects on Amorphous Calcium Carbonate (ACC) Structure, Stability, and Crystallization. *Adv. Funct. Mater.* **25**, 3081–3090.

Tomita Y., Ando T. and Ueno K. (1965) Infrared Spectra of Nitrilotriacetate Chelates in Aqueous Solution. *J. Phys. Chem.* **69**, 404–407.

Viani A., Mácová P., Ševčík R. and Zárybnická L. (2022a) Mechanism of magnesium phosphate cement retardation by citric acid. *Ceram. Int.*

Viani A., Zárybnická L., Ševčík R., Mácová P., Machotová J. and Veltruská K. (2022b) Struvite-K crystal growth inhibition by citric acid: Formation of complexes in solution and surface adsorption effects. *J. Cryst. Growth* **598**, 126858.

Wada N., Kanamura K. and Umegaki T. (2001) Effects of Carboxylic Acids on the Crystallization of Calcium Carbonate. *J. Colloid Interface Sci.* **233**, 65–72.

Wang Y., Grenabo L., Hedelin H., McLean R. J. C., Curtis Nickel J. and Pettersson S. (1993) Citrate and urease-induced crystallization in synthetic and human urine. *Urol. Res.* **21**, 109–115.

Westin K.-J. and Rasmuson Å. C. (2005) Nucleation of calcium carbonate in presence of citric acid,

DTPA, EDTA and pyromellitic acid. *J. Colloid Interface Sci.* **282**, 370–379.

Wierzbicki A., Sallis J. D., Stevens E. D., Smith M. and Sikes C. S. (1997) Crystal Growth and Molecular Modeling Studies of Inhibition of Struvite by Phosphocitrate. *Calcif. Tissue Int.* **61**, 216–222.

Wilson A. and Nicholson J. W. (1993) *Acid-base cements*., Cambridge University Press.

Xu H., Guo L., Zhao Y., Gao M., Jin C., Ji J. and She Z. (2021) Accelerating phosphorus release from waste activated sludge by nitrilotriacetic acid addition during anaerobic fermentation process and struvite recovery. *Process Saf. Environ. Prot.* **147**, 1066–1076.

Zárybnická L., Mácová P. and Viani A. (2022) Properties enhancement of magnesium phosphate cement by cross-linked polyvinyl alcohol. *Ceram. Int.* **48**, 1947–1955.

Zhang C., Xu K., Zheng M., Li J. and Wang C. (2018) Factors Affecting the Crystal Size of Struvite-K Formed in Synthetic Urine Using a Stirred Reactor. *Ind. Eng. Chem. Res.* **57**, 17301–17309.